Modelling the Impact of Mass Transport in a Miniplant Photoreactor

Florian Gaulhofer,[†] Henning Becker,[†] Alexander Peschl,[‡] and Dirk Ziegenbalg[*,†]

†*Institute of Chemical Engineering, Ulm University, Albert-Einstein-Allee 11, 89081 Ulm, Germany.*

‡*Peschl Ultraviolet GmbH, Weberstraße 19, 55130 Mainz, Germany.*

E-mail: dirk.ziegenbalg@uni-ulm.de

Supporting Information

1 Experimental

1.1 Chemicals

1,3,3-trimethylindolino-6'-nitrobenzopyrylospirane (CAS: 1498-88-0, $M = 322.36\,\mathrm{g\,mol^{-1}}$, 6-NO2-BIPS) was purchased from *TCI Development Co., Ltd*. Technical grade ethanol (96 vol%, TechniSolv™) from *VWR International Ltd* and analytical grade ethanol (99.5 vol%, EMPLURA™, Supelco™) from *Merck* were used as solvent. The spiropyrane powder was dissolved in ethanol with a Palssonic PTIC-10-ES ultrasonic bath (*ALLPAX GmbH*, Germany).

1.2 Analytical methods

Online UV/vis spectroscopy was conducted with a balanced deuterium halogen lamp AvaLight-DH-S-BAL, two fibres FC-UV600-2-BX, and a AvaSpec-ULS2048 spectrometer (all *Avantes*

BV, Netherlands). Self-designed mounts for the optical fibres were used as measuring cells and fitted to the process tube.[1] The reaction was monitored at a wavelength $\lambda_{obs} = 540\,nm$, which is characterisitic for species **2**.

1.3 Capillary reactor

Experimental setup

A capillary reactor made of fluorinated ethylene propylene (FEP) with an inner diameter of $1.5875\,mm$ and outer diameter of $3.175\,mm$ (*Bohlender GmbH*, Germany) was used to conduct the photoisomerization.[2] The irradiated volume V of the reactor was $0.98\,mL$. A 3D-printed mount (s. Fig. S1 a, b) ensured a tight side-by-side arrangement of the capillary with a defined circular irradiated area. An UV LED (SMD-LED NVSU233A, *Nichia Co.*, Japan) was used and operated at a voltage U of $3.75\,V$ and currents I of 50 to 200 mA, resulting in emitted photon fluxes q_p^{em} of 0.07×10^{-2} to $0.3\,\mu mol\,s^{-1}$. The emitted photon flux was only linear dependent on the current for currents of $I < 200\,mA$ (s. Fig. S2 b). The LED heat sink was snapped to the top of the capillary bed (s. Fig. S1 c). The external photonic efficiency of this setup was previously determined by radiometry and actinometry as $\eta_{sys} = 0.54$ and thus used to calculate the photon flux incident on the reaction solution.[3,4] The used diaphragm dosing pump SIMDOS 10 (*KNF Flodos AG*, Germany) provided flow rates of 10 to 100 $mL\,min^{-1}$, correlating to Reynolds numbers Re of 130 to 1400.

Experimental procedure

The reaction solution was pumped from a reservoir through the capillary reactor into a vessel, and online UV/vis spectroscopy was conducted at the outlet of the reactor with an UV/vis measuring cell. While pumping with a constant flow rate $\dot{V}$, the operating current I for the LED was increased and each condition was held for $8\,s$, during which a constant concentration $c_2(\dot{V}, I)$ was registered by UV/vis spectroscopy at $540\,nm$. Experiments were conducted at ambient temperature ($T_{am} = 21\,°C$) and fresh solutions were equilibrated overnight to ensure thermal equilibrium between species **1** and **2**.
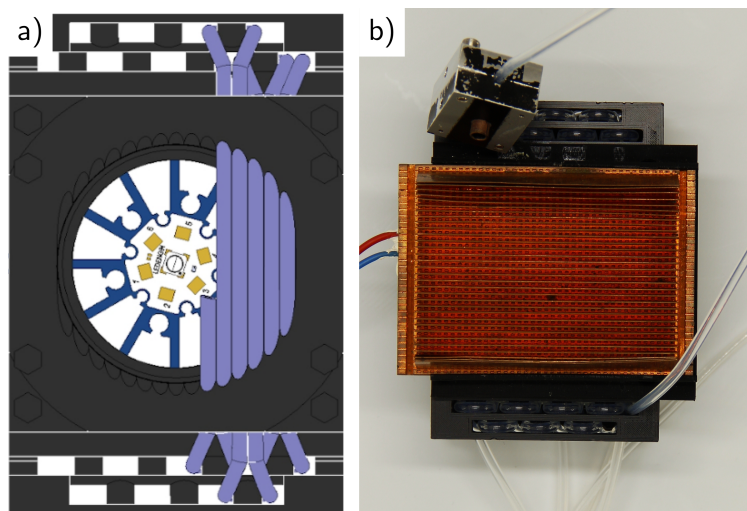
Figure S1 a) Schematic view of the capillary reactor, b) picture of reactor without LED and c) with mounted UV LED.

Experimentally the conversion X_1 of **1** of the photoisomerization is calculated from the measured decadic absorbance A_{obs} at the observation wavelength ($\lambda_{\mathrm{obs}} = 540\,\mathrm{nm}$) as follows:

$$X_1(t_{\mathrm{r}}) = \frac{1}{c_{1,0}} \frac{A_{\mathrm{obs}}(t_{\mathrm{r}}) \cdot \ln(10)}{\kappa_2(\lambda_{\mathrm{obs}}) \cdot s}, \tag{S1}$$

with the Napierian absorption coefficient κ_2 and the optical pathlength s of the capillary ($s = d_i$). Experimental data for the estimation of the quantum yield Φ by parameter fitting is presented in Tab. S1 and S2.

Table S1 Experimental absorbance A measured at reaction times t_r in the capillary reactor for a concentration of $c_{1,0} = 3.102\,\mathrm{mol\,m^3}$ and fitted parameter Φ for each incident photon flux q_p.

$c_{1,0}$ / $\mathrm{mol\,m^{-3}}$	3.102			
q_p / $\mu\mathrm{mol\,s^{-1}}$	0.07	0.1	0.14	0.3
t_r / s	A / 1			
0.0	0.239			
0.587	0.259	0.268	0.271	0.323
0.587	0.26	0.269	0.282	0.324
0.620	0.255	0.264	0.279	0.325
0.620	0.26	0.27	0.285	0.33
0.620	0.26	0.269	0.284	0.33
0.699	0.258	0.269	0.285	0.34
0.699	0.262	0.273	0.288	0.341
0.746	0.265	0.276	0.293	0.346
Φ	0.141	0.146	0.149	0.148

Table S2 Experimental absorbance A measured at reaction times t_r in the capillary reactor for a concentration of $c_{1,0} = 2.1714\,\mathrm{mol\,m^3}$ and fitted parameter Φ for each incident photon flux q_p.

$c_{1,0}$ / $\mathrm{mol\,m^{-3}}$	2.1714			
q_p / $\mu\mathrm{mol\,s^{-1}}$	0.07	0.1	0.14	0.3
t_r / s	A / 1			
0.0	0.112			
0.557	0.131	0.14	0.153	0.195
0.557	0.133	0.142	0.154	0.196
0.587	0.129	0.138	0.153	0.197
0.587	0.13	0.139	0.153	0.197
0.620	0.134	0.144	0.157	0.205
0.620	0.135	0.144	0.158	0.206
0.699	0.134	0.145	0.162	0.216
0.699	0.135	0.146	0.162	0.215
Φ	0.138	0.143	0.144	0.145

1.4 LED data

The UV LED (SMD-LED NVSU233A, *Nichia Co.*, Japan) was glued to a cuboid heat sink (s. Fig. S2 a). With increasing electrical current, the efficiency of emitting photons is reduced due to overheating of the LED (s. Fig. S2 b). A regression line (solid) of the first five data points shows a linear dependency of electrical current I up to $300\,\mathrm{mA}$ for the measured

relative irradiance E_{rel}. Hence, only data points for electrical currents I in the range of 50 to 200 mA were considered for the determination of the quantum yield.
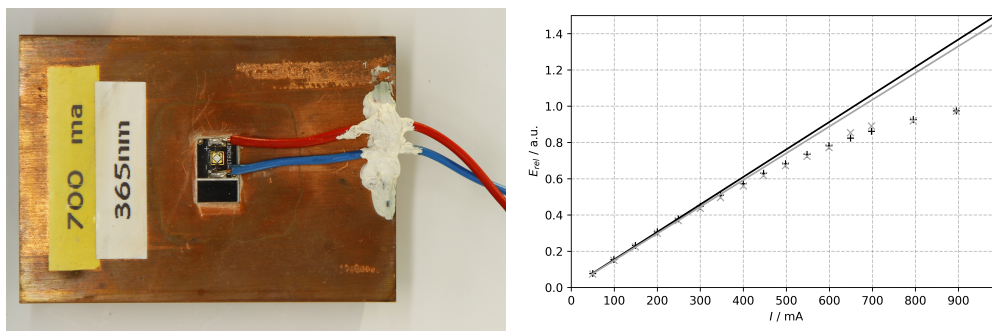

Figure S2 a) LED with cuboid heat sink used as light source in the capillary reactor. b) Two measurements (black, grey) of the irradiance E_{rel} at the surface of the LED with Power Meter Model 1936-R (Newport, US).
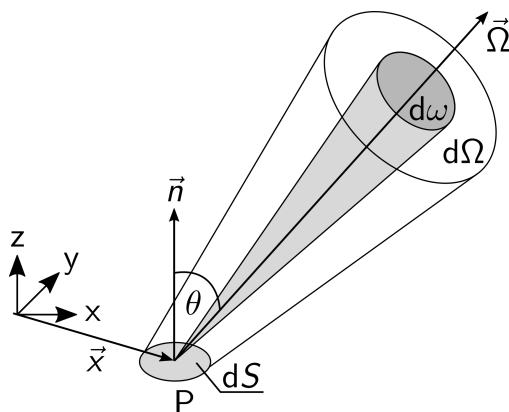
2 Theoretical Methods

2.1 Photon transport

Figure S3 Schematic representation of a bundle of rays (photons) characterizing the radiation field. Adopted from Cassano et al..[5]

Fig. S3 shows the propagation of radiant energy (photons), represented by bundles of rays with a given energy, schematically. The rays are described by the incident spectral radiance (specific spectral intensity), which is the fundamental property for characterizing radiation fields. dS is an arbitrarily oriented small area with the spatial coordinate $\vec{x}$, P a

point in this area, and $\vec{n}$ the normal to the area at point P. At a given time, rays will pass through this area element in all directions.

A balance of all incoming and outgoing fluxes through this balance element requires constitutive relations to describe phenomena such as absorption, emission, and in/out scattering. A specific direction $\vec{\Omega}$ coincides with the axis of an elementary cone of solid angle $d\Omega$ and $\vec{\Omega}$ is characterized by the unit direction vector $\vec{\Omega}$ with the angle θ to the normal $\vec{n}$.

All elementary solid angles, corresponding to rays parallel to the direction $\vec{\Omega}$ passing through dS, define a truncated semi-infinite cone $d\omega$, having a cross-sectional area perpendicular to the point P $dS\cos\theta$. dE_λ is the total amount of radiant energy passing through the area dS, inside the cone in the time dt, and with an energy of the wavelength range between λ and $\lambda + d\lambda$. The incident spectral radiance is defined as:[5,6]

$$L_{\lambda,\vec{\Omega}}(t,\vec{x}) = \lim_{dA,d\Omega,dt,d\lambda \to 0} \frac{dE_\lambda}{dA\cos\theta d\Omega dt d\lambda} \tag{S2}$$

There is no fundamental difference between incident spectral radiance L_λ or incident photon flux density $L_{p,\lambda}$, as the unit conversion is a constant:

$$L_{p,\lambda} = L_\lambda \cdot \frac{\lambda}{N_A \cdot h \cdot c}, \tag{S3}$$

with the wavelength of the photon λ, the Avogadro constant N_A, the Planck's constant h, and the speed of light c.

The spectral photon fluence rate $E_{p,o,\lambda}$ (overall, o) is the integral over the solid angle Ω of the spectral photon flux density $L_{p,\lambda}(\vec{x},t)$ incident from all directions onto a small sphere, divided by the cross-sectional area of that sphere:

$$E_{p,o,\lambda}(\vec{x},t) = \int_{\Omega=4\pi} L_{p,\lambda,\Omega}(\vec{x},t)d\lambda\, d\Omega. \tag{S4}$$

The spectral photon flux density $L_{p,\lambda,\Omega}(\vec{x},t)$ is obtained from the photon transport equation.

The photon transport equation for a homogeneous medium for absorption without scattering and emission effects is expressed as:[5,7–9]

$$\frac{dL_{p,\lambda,\Omega}(\vec{x},t)}{ds} = -\alpha L_{p,\lambda,\Omega}(\vec{x},t) , \tag{S5}$$

where $\frac{dL_{p,\lambda,\Omega}(\vec{x},t)}{ds}$ is the directional derivative along the direction s at a point $\vec{x}$ in the reaction space of the incident photon flux density. The spectral linear Napierian absorption coefficient α_λ is expressed according to Eq. 4. Note, in case of the isomerization of spiropyrane, both species **1** and **2** absorb photons at λ_{irr} ((s. Eq.4, $I = 2$).

Integrating the incident photon flux density $L_{p,\lambda,\Omega}(\vec{x},t)$ (s. Eq. S5) over all directions Ω, and inserting the expression for the fluence rate (s. Eq. 5) results in an integro-differential equation:

$$\frac{dL_{p,\lambda}(\vec{x},t)}{ds} = -\int_{\Omega=4\pi} \alpha_\lambda L_{p,\lambda,\Omega}(\vec{x},t)\,d\Omega = -\alpha E_{p,o,\lambda}(\vec{x},t) \tag{S6}$$

Solving the integro-differential problem in a six-dimensional Euclidean space needs sophisticated numerical methods.[10] The most widespread numerical methods used to solve the 3D radiative transport equation (RTE) are the Discrete Ordinate method (DOM) and the Monte Carlo method.[9,11–14]

Assuming monochromatic light spectral properties, such as $E_{p,o,\lambda}(\vec{x},t)$ and the $L_{p,\lambda}(\vec{x},t)$, are integrated over a single wavelength λ_1 and reduced in the spectral dimension as follows:

$$E_{p,o}(\vec{x},t) = \int_{\lambda_1}^{\lambda_1} E_{p,o,\lambda}\,d\lambda \tag{S7}$$

$$L_p(\vec{x},t) = \int_{\lambda_1}^{\lambda_1} L_{p,\lambda}(\vec{x},t)\,d\lambda . \tag{S8}$$

For a one-dimensional, collimated ($\vec{x} = x$) monochromatic beam of radiation, the Beer-

Lambert law along the x-direction ($\vec{x} = x$) is most commonly used and expressed by the fluence rate $E_{p,o}(x)$ as follows:

$$E_{p,o}(x) = E_{p,o}^0 \exp(-\alpha x), \tag{S9}$$

with the linear absorption coefficient α of the solution (s. Eq.4, $I = 2$).

2.2 Derivation of the working equation for rectangular photoreactors

The Beer-Lambert law is an analytical solution of the RTE for collimated light propagation and is written as for two absorbing species 1 and 2 at the wavelength $\lambda = 365 \, \text{nm}$:

$$\frac{dE_p}{dx} = -\alpha E_p = -(\kappa_1 c_1 + \kappa_2 c_2) E_p \tag{S10}$$

Solving the differential equation by separating the variables leads to the relation for the photon irradiance E_p as a function of x:

$$\ln\left(\frac{E_p}{E_p^0}\right) = -(\kappa_1 c_1 + \kappa_2 c_2) x \tag{S11}$$

Introduction of the following model parameters:

$$A_e^0 = c_{1,0} \cdot (\kappa_1 + \kappa_2) \cdot s, \tag{S12}$$

$$\beta_1 = \frac{\kappa_1}{\kappa_1 + \kappa_2}, \tag{S13}$$

$$X_1 = 1 - \frac{c_1}{c_{1,0}} \tag{S14}$$

and then inserting the model parameters into the expression for the photon irradiance $E_p(x)$ gives:

$$E_p(x) = E_p^0 \cdot \exp\left(-\frac{A_e^0}{s}[(1 - X_1)\beta_1 + (1 - \beta_1)X_1]x\right). \tag{S15}$$

Based on the kinetics approach according to Eq. 1, the explicit expression for the AVRPA $\langle L_p^a \rangle$ is written:

$$\langle L_p^a(\vec{x},t) \rangle = \frac{1}{V} \int_V L_p^a \, dV = \frac{1}{V} \int_V \alpha L_p \, dV = \frac{1}{V} \int_V \alpha E_p \, dV \tag{S16}$$

Assuming collimated light propagation, the quantities photon flux density L_p and irradiance E_p are equal. Inserting the explicit expression for the photon irradiance E_p into the kinetics approach for collimated light propagation results in the following expression for the AVRPA:

$$\langle L_p^a(x,t) \rangle = \frac{1}{V} \int_V \kappa_1 c_1 E_p^0 \cdot \exp\left(-\frac{A_e^0}{s}[(1-X_1)\beta_1 + (1-\beta_1)X_1]x\right) dV \tag{S17}$$

Integration over the volume $dV = S_{irr} \cdot dx$ along the x-direction within the boundaries $x = 0$ and $x = s$ results in the following expression:

$$\langle L_p^a \rangle = \frac{S_{irr}}{V} \kappa_1 c_1 E_p^0 \int_0^s \cdot \exp\left(-\frac{A_e^0}{s}[(1-X_1)\beta_1 + (1-\beta_1)X_1]x\right) dx \tag{S18}$$

$$= \frac{S_{irr}}{V} \frac{\kappa_1 c_1 E_p^0}{-\frac{A_e^0}{s}[(1-X_1)\beta_1 + (1-\beta_1)X_1]} \cdot \left[\exp\left(-\frac{A_e^0}{s}[(1-X_1)\beta_1 + (1-\beta_1)X_1]x\right)\right]_0^s \tag{S19}$$

$$= \frac{S_{irr}}{V} \frac{\kappa_1 c_1 E_p^0}{\frac{A_e^0}{s}[(1-X_1)\beta_1 + (1-\beta_1)X_1]} \cdot \left[1 - \exp\left(-A_e^0[(1-X_1)\beta_1 + (1-\beta_1)X_1]\right)\right] \tag{S20}$$

The introduction of f as absorption factor/photokinetic factor:

$$f = \frac{\beta_1(1-X_1)}{(1-X_1)\beta_1 + (1-\beta_1)X_1} \cdot \left[1 - \exp\left(-A_e^0[(1-X_1)\beta_1 + (1-\beta_1)X_1]\right)\right] \tag{S21}$$

is used to write the expression of the AVRPA for a rectangular geometry:

$$\langle L_p^a \rangle = \frac{E_p^0}{s} f. \tag{S22}$$

Transferring the AVRPA to a reactor system, for example a batch stirred tank reactor (BSTR), results in the following material balance for species 1:

$$\frac{dc_1}{dt} = -r_p = -\Phi \langle L_p^a \rangle = -\Phi \frac{E_p^0}{s} f. \tag{S23}$$

Based on the definition of conversion X_1, the following applies:

$$\frac{dX_1}{dt} = \Phi \cdot \frac{1}{c_{1,0}} \frac{E_p^0}{s} \cdot f = \Phi \cdot \frac{1}{c_{1,0}} \frac{q_p^0}{V} \cdot f. \tag{S24}$$

2.3   Calculation of the diffusion coefficient

The diffusion coefficient D_m in units $\mathrm{cm^2\,s^{-1}}$ of a molecule dissolved in a solvent of viscosity η in unit mPa ($\eta = 1.17$ mPa) and molecular weight M_{sol} in unit $\mathrm{g\,mol^{-1}}$ ($M_{\mathrm{sol}} = 46.07$ $\mathrm{g\,mol^{-1}}$) is estimated by the empirical WILKE-CHANG equation:

$$D_m = \frac{7.12 \times 10^{-8} \cdot \sqrt{\Psi \cdot MW_{\mathrm{sol}}}}{\eta \cdot V^{0.6}} \cdot T \tag{S25}$$

with the interaction factor of ethanol ($\Psi = 1.5$), the molar volume V of 6-NO2-BIPS in units $\mathrm{cm^3\,mol^{-1}}$ ($V = 403$ $\mathrm{cm^3\,mol^{-1}}$) and temperature in unit K ($T = 293.15$ K). The diffusion coefficient of 6-NO2-BIPS in ethanol is calculated as $D = 0.421 \times 10^{-9}\,\mathrm{m^2\,s^{-1}}$.

2.4   Numerical implementation of the 2Dt model

The convection-diffusion-reaction system (s. Eq. 6) is a parabolic partial differential equation (PDE). The PDE is transformed into a system of ordinary differential equations (ODE) by a semi-discretization (method of lines) of spatial coordinates x and y. The numerical solution of the ODE system is obtained by an implicit multi-step variable-order (1 to 5) method based on a backward differentiation formula for the derivative approximation.[15]
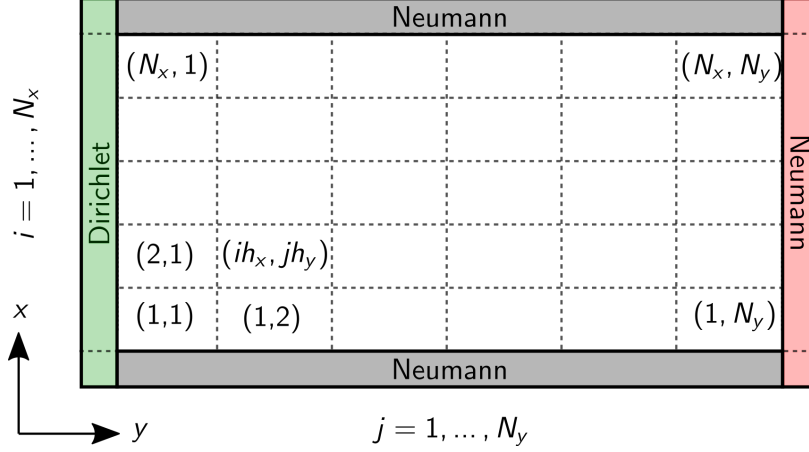
Figure S4 Representation of the grid in x and y direction with boundary conditions of the concentration.

The numerical scheme is written as:

$$\underline{B} \cdot \vec{\dot{y}} = \vec{f}(t, \vec{y}), \qquad \vec{y}(t_0) = \vec{y}_0. \tag{S26}$$

With $\underline{B} \in \mathbb{R}^{n \times n}$ as a nonsingular and sparse matrix, the time derivative of the state variable $\vec{\dot{y}} \in \mathbb{R}^n$, and the right-hand side $\vec{f}(t, \vec{y}) \in \mathbb{R}^n$. The dimension of n depends on the number of grid points in x- and y-direction. A regular grid in x and y direction is defined (s. Fig. S4):

$$G = \begin{cases} (ih_x \, jh_y) \mid & i = 0, \ldots, N_x, h_x = \frac{1}{N_x + 2}, \\ & j = 0, \ldots, N_y, h_y = \frac{1}{N_y + 2}. \end{cases} \tag{S27}$$

with the spatial step size h_x, h_y in x and y direction. The total number of grid points is $N_{tg} = (N_x + 2) \times (N_y + 2)$, and the number of the inner grid points is $N_{ig} = N_x \times N_y$.

The right-hand side $\vec{f}(t, \vec{y})$ consists of contributions of the convection term $\underline{C}$, the dispersion term $\underline{D}$, and the reaction term $\underline{R}$:

$$\vec{f}(t, \vec{y}) = -\underline{C}_y(t, \vec{y}) + \underline{D}_y(t, \vec{y}) + \underline{D}_x(t, \vec{y}) + \underline{R}(t, \vec{y}). \tag{S28}$$

The discretization of the convection term in y direction is approximated by a single point

upward differentiation scheme (SPUDS) of 1. order, and accuracy of 2. order. The discretization of the dispersion terms in x and y direction are approximated by a central finite differences scheme (CD) of 2. order, and accuracy of 2. order. The stencil of the spatial derivative of the state variable y is formulated as:

$$
\begin{aligned}
\left(\frac{\partial y}{\partial y}\right)_j^{SPUDS} &= \frac{2y_{j+1} + 3y_j - 6y_{j-1} + y_{j-2}}{6h_y} \ , \ j = 2, \ldots, N_y - 1 \\
\left(\frac{\partial^2 y}{\partial y^2}\right)_j^{CD} &= \frac{-y_{j+2} + 16y_{j+1} - 30y_j + 16y_{j-1} - y_{j-2}}{12h_y^2} \ , \ j = 2, \ldots, N_y - 1 \\
\left(\frac{\partial^2 y}{\partial x^2}\right)_i^{CD} &= \frac{-y_{i+2} + 16y_{i+1} - 30y_i + 16y_{i-1} - y_{i-2}}{12h_x^2} \ , \ i = 2, \ldots, N_x - 1 \ .
\end{aligned}
\tag{S29}
$$

The contribution of the source/reaction term $\underline{R}(t, \vec{y})$ is a function of the radiation field (s. Eq. 9). The RTE is solved for every time-step inside the numerical integration of the higher-level (parent) system of ODEs, as an additional subsystem of ODEs. For every time step of the parent system of ODEs, the updated concentration field is interpolated along x-direction, and passed to the subsystem. The subsystem is solved as a simple boundary value problem with the explicit Runge-Kutta method of 4. order.[16] Numerics were implemented in Python with the packages: NumPy, and SciPy.[17–19]

2.5 Grid study of the 2Dt capillary photoreactor model

Fig. S5 shows the grid study of the capillary photoreactor for 5 grids: i) 15x10, and ii) 20x30, ii) 40x30, iv) 80x30 and v) 80x60. The grid study was performed for the following case: $D_x = \frac{u \cdot L}{\text{Bo}}, D_y = D_m, u = u_0$ with a collimation factor of $\Lambda = 1$. The grid is most sensitive in the x direction and correlates with the numerical gradient of the underlying physical conditions of the photochemical model. The other cases of the parameter study create different numerical gradients and to account for the variation of the parameter study, a grid of size 80x60 was chosen for all computations presented. An average calculation time of a single operation point (80x60) of $138\,\text{s}$ was found. The python code has been executed on an AMD® Ryzen™ 5 3600 processor with $16\,\text{GB}$ RAM running a Windows 10
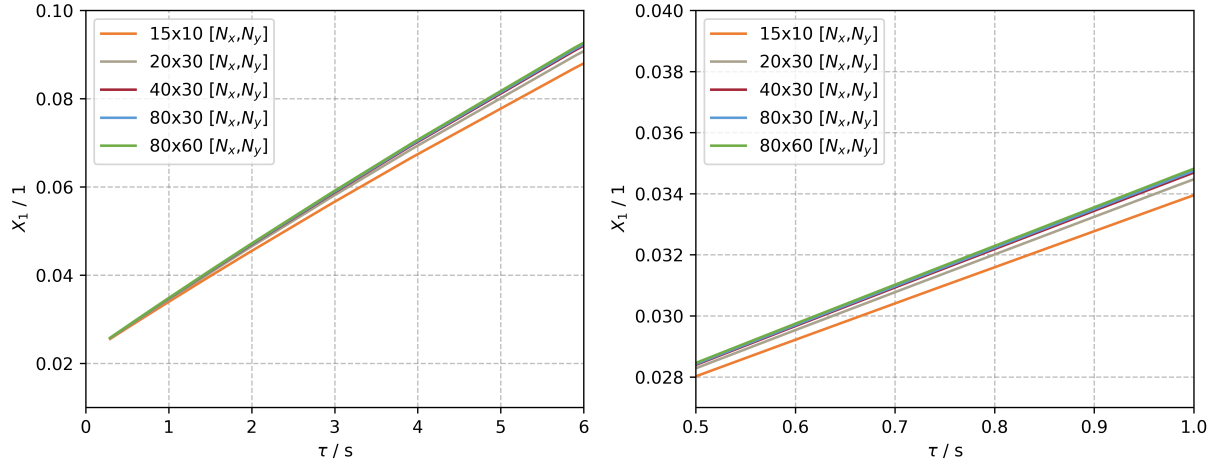
Figure S5 Study of spatial discretization in x (N_x) and y (N_y) direction for the conversion X_1 in the capillary photoreactor.

Professional operating system.

2.6 Grid study of the 2Dt MISCOP model

A grid sensitivity analysis was conducted for the MISCOP system in the SMX10 configuration at a flow rate of $\dot{V} = 4\,\mathrm{L\,min}^{-1}$. The parameter study for the transverse dispersion coefficient D_x was carried out at 18 positions. Fig. S6 shows two intervals for D_x (1×10^{-10} to 1×10^{-2} and 1×10^{-6} to 1×10^{-4}) for two light source powers: a) $P_{\mathrm{LED}} = 100\,\%$ and b) $P_{\mathrm{LED}} = 35\,\%$.

At a power of $P_{\mathrm{LED}} = 100\,\%$, a grid size of 80x40 is sufficiently accurate to obtain precise solutions of X_1 along a dispersion coefficient range of $1 \times 10^{-10}\,\mathrm{m^2\,s^{-1}}$ to $1 \times 10^{-2}\,\mathrm{m^2\,s^{-1}}$ (s. Fig. S6 a). The solution shows the greatest sensitivity to grid point variation at very high transverse dispersion coefficients. Increasing the axial discretization N_x does not further improve the accuracy of the solution. The average difference in the numerical solution between a grid size of 100x50 and a grid size of 80x40 across all 18 calculation points is $\delta\bar{X}_1 = 9.4 \times 10^{-4}$, which is sufficiently accurate.

A reduction in power to $P_{\mathrm{LED}} = 35\,\%$ shows the same result (s. Fig. S6 b). Here, too, a grid size of 80x40 is sufficiently accurate, with an average difference of $\delta\bar{X}_1 = 4.4 \times 10^{-4}$
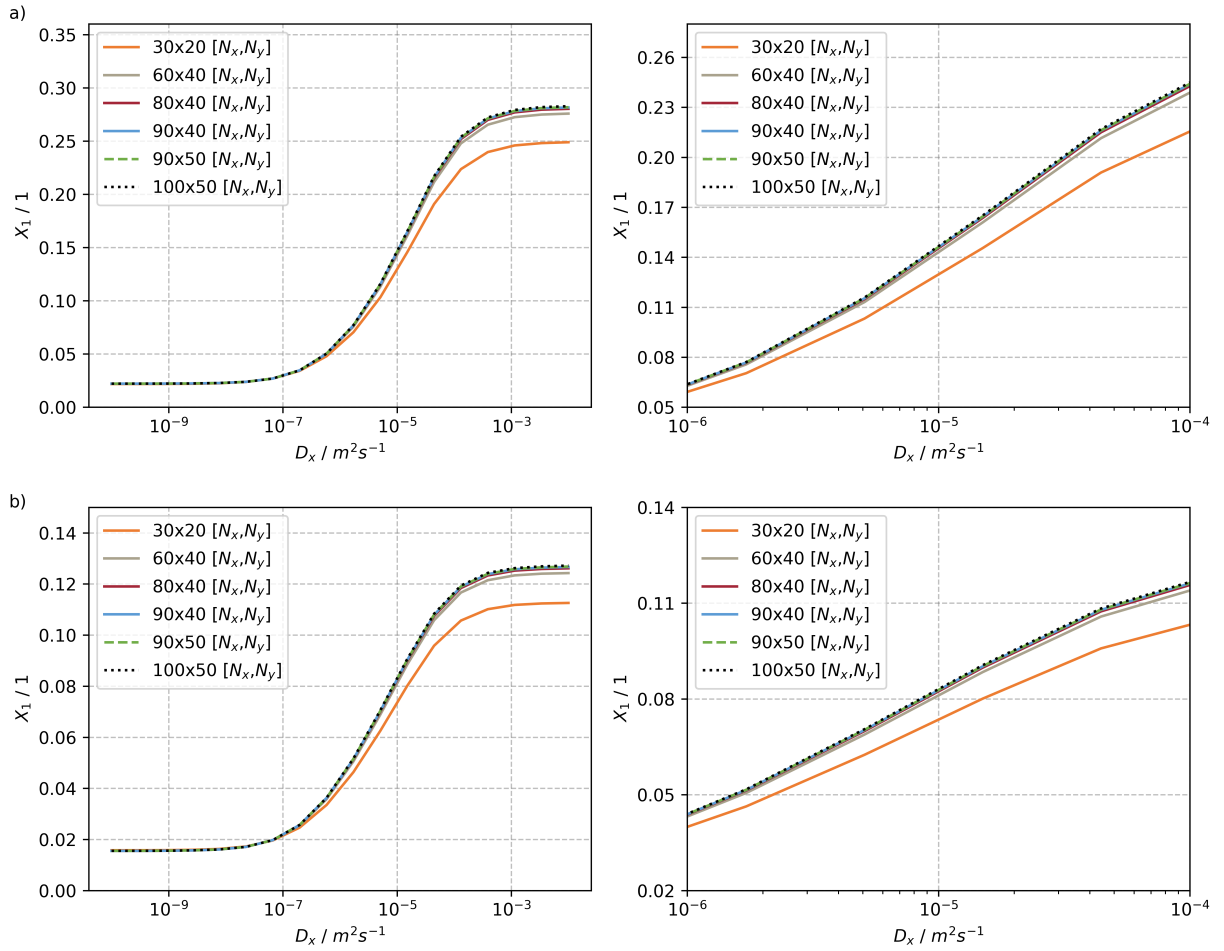
S13

Figure S6 Investigation of spatial discretization in the x (N_x) and y (N_y) directions for the conversion X_1 of the SMX variant of the MISCOP system for two irradiation cases: a) $P_{\mathrm{LED}} = 100\%$, and b) $P_{\mathrm{LED}} = 35\%$.

compared to a grid size of 100x50. For all presented calculations, a grid size of 80x40 was chosen. The computation time for a single operating point depends on the numerical gradients. On average, the calculation time was $t_{calc} \approx 121\,\mathrm{s}$ (80x40) per operating point. The Python code was executed for the parameter studies on an Intel® Core™ i9 10900 processor with 32 GB of RAM and a "Windows 10 Professional" operating system.
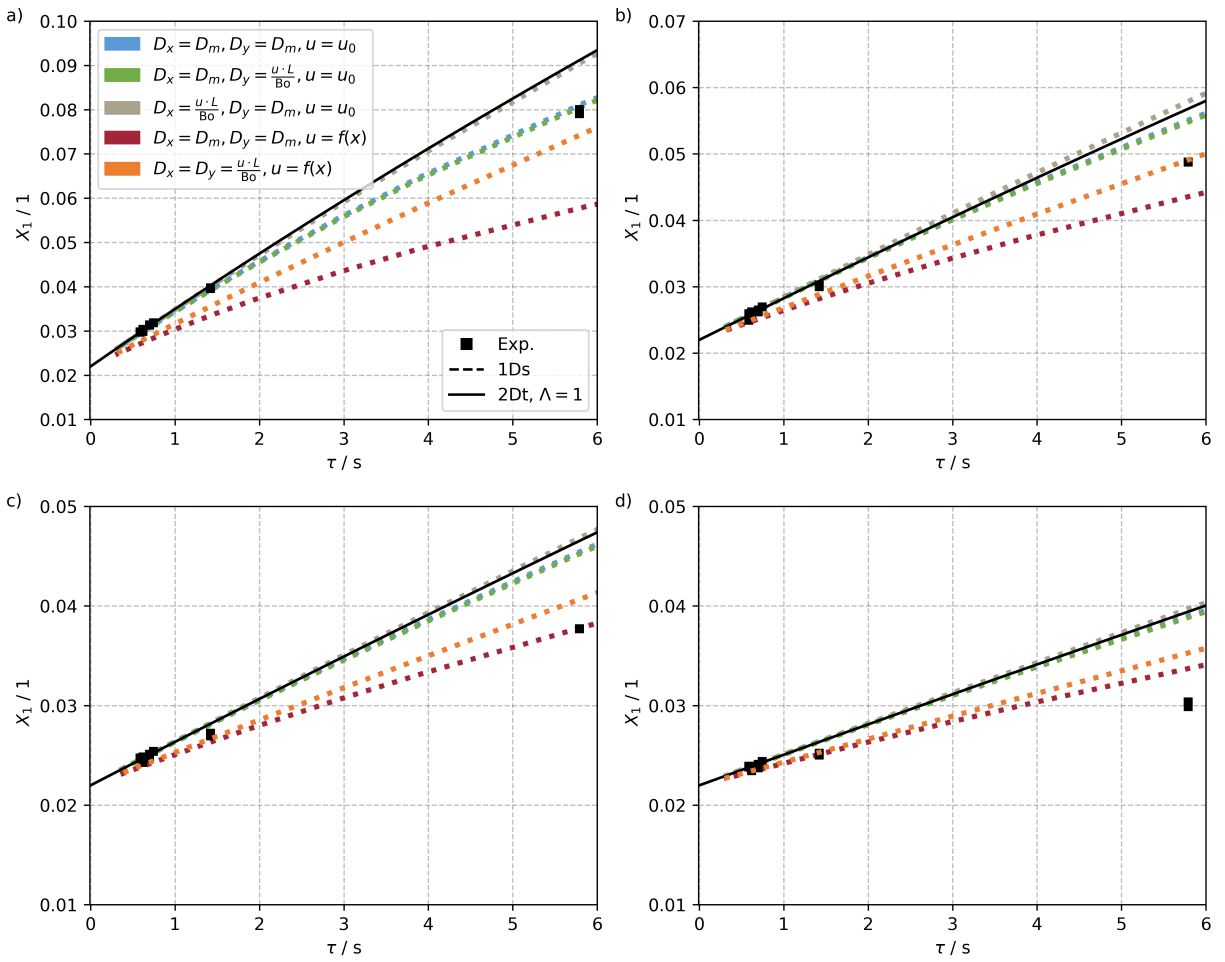
3 Additional results

Figure S7 Results of the case study of the capillary photoreactor for a collimation factor of $\Lambda = 1$ at: a) $q_{\mathrm{p}}^0 = 0.30\,\mu\mathrm{mol\,s^{-1}}$, b) $q_{\mathrm{p}}^0 = 0.14\,\mu\mathrm{mol\,s^{-1}}$, c) $q_{\mathrm{p}}^0 = 0.10\,\mu\mathrm{mol\,s^{-1}}$ and d) $q_{\mathrm{p}}^0 = 0.07\,\mu\mathrm{mol\,s^{-1}}$.
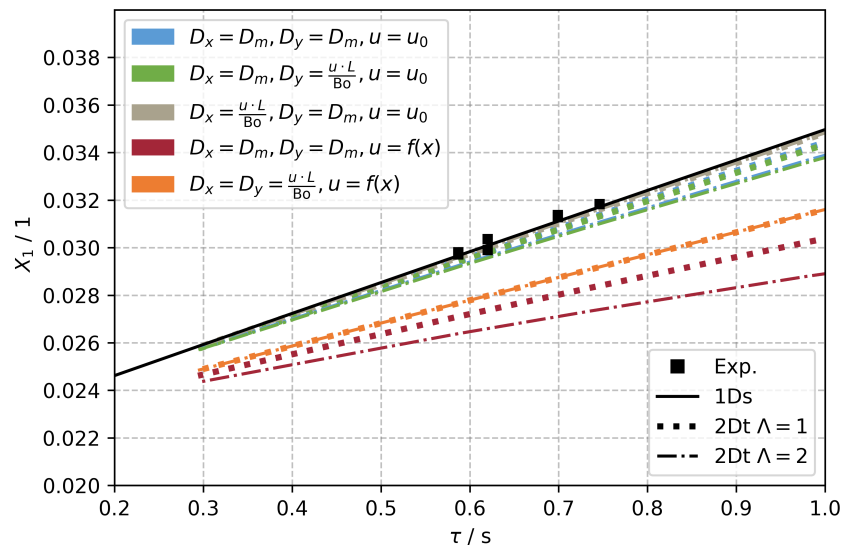
Figure S8 Results of the case study of the capillary photoreactor for a collimation factor of $\Lambda = 1$ for residence times below $1\,\mathrm{s}$.

References

(1) Ümit Taştan; Dollinger, J.; Ziegenbalg, D. Measurement of UV/VIS-absorption spectra of photochemically active solutions in continuous flow. Flow Measurement and Instrumentation **2018**, <u>59</u>, 211–214.

(2) Sender, M.; Ziegenbalg, D. Radiometric measurement techniques for in-depth characterization of photoreactors – part 2: 3 dimensional and integral radiometry. Reaction Chemistry & Engineering **2021**, <u>6</u>, 1614–1627.

(3) Wriedt, B.; Ziegenbalg, D. Common pitfalls in chemical actinometry. Journal of Flow Chemistry **2020**, <u>10</u>, 295–306.

(4) Sender, M.; Wriedt, B.; Ziegenbalg, D. Radiometric measurement techniques for in-depth characterization of photoreactors – part 1: 2 dimensional radiometry. Reaction Chemistry & Engineering **2021**, <u>6</u>, 1601–1613.

(5) Cassano, A. E.; Martin, C. A.; Brandi, R. J.; Alfano, O. M. Photoreactor analysis and design: fundamentals and applications. Industrial & Engineering Chemistry Research **1995**, <u>34</u>, 2155–2201.

(6) Ziegenbalg, D. Heterogeneous Photocatalysis; John Wiley & Sons, Ltd, 2021; Chapter 7, pp 155–186.

(7) Vincenti, W. G.; Kruger, C. H. Introduction to Physical Gas Dynamics. Journal of the Royal Aeronautical Society **1966**, <u>70</u>, 741–742.

(8) Braslavsky, S. E.; Braun, A. M.; Cassano, A. E.; Emeline, A. V.; Litter, M. I.; Palmisano, L.; Parmon, V. N.; Serpone, N. Glossary of terms used in photocatalysis and radiation catalysis (IUPAC Recommendations 2011). Pure and Applied Chemistry **2011**, <u>83</u>, 931–1014.

(9) Moreno, J.; Casado, C.; Marugán, J. Improved discrete ordinate method for accurate simulation radiation transport using solar and LED light sources. Chemical Engineering Science **2019**, _205_, 151–164.

(10) Cornet, J.-F.; Dussap, C.; Gros, J.-B.; Binois, C.; Lasseur, C. A simplified monodimensional approach for modeling coupling between radiant light transfer and growth kinetics in photobioreactors. Chemical Engineering Science **1995**, _50_, 1489–1500.

(11) Chandrasekhar, S. Radiative Transfer Clarendon Press. 1950.

(12) Carlson, B. G. Transport Theory: Discrete Ordinates Quadrature Over the Unit Sphere.; 1970.

(13) Lathrop, K. D. Use of Discrete-Ordinates Methods for Solution of Photon Transport Problems. Nuclear Science and Engineering **1966**, _24_, 381–388.

(14) Fiveland, W. A. Discrete-Ordinates Solutions of the Radiative Transport Equation for Rectangular Enclosures. Journal of Heat Transfer **1984**, _106_, 699–706.

(15) Shampine, L. F.; Reichelt, M. W. The MATLAB ODE Suite. SIAM Journal on Scientific Computing **1997**, _18_, 1–22.

(16) Dormand, J.; Prince, P. A family of embedded Runge-Kutta formulae. Journal of Computational and Applied Mathematics **1980**, _6_, 19–26.

(17) Van Rossum, G.; Drake, F. L. Python 3 Reference Manual; CreateSpace: Scotts Valley, CA, 2009.

(18) Harris, C. R. et al. Array programming with NumPy. Nature **2020**, _585_, 357–362.

(19) Virtanen, P. et al. SciPy 1.0: fundamental algorithms for scientific computing in Python. Nature Methods **2020**, _17_, 261–272.